Supplementary Information (SI) for Journal of Materials Chemistry C.

Supplementary Material for:

Assessing the influence of nanoscale morphology on the mechanical properties of semiconducting polymers

Silvia Cristofaro[1,2], Dorothée Brandt[1], Vincent Lemaur[3], Ki-Hwan Hwang[4,5], Ljiljana Fruk[5], Deepak Venkateshvaran[4,5], Luca Muccioli[2], Silvia Orlandi[2] and Yoann Olivier[2]

[1] *Laboratory for Computational Modeling of Functional Materials & Solid State Physics Laboratory, Namur Institute of Structured Matter, University of Namur, Rue de Bruxelles, 61, 5000 Namur, Belgium*

[2] *Dipartimento di Chimica Industriale "Toso Montanari" Università di Bologna, Via Piero Gobetti 85, 40126 Bologna, Italy*

[3] *Laboratory for Chemistry of Novel Materials, University of Mons, Place du Parc, 20, B-7000 Mons, Belgium*

[4] *Cavendish Laboratory, University of Cambridge, JJ Thomson Avenue, Cambridge, CB3 0HE, United Kingdom*

[5] *Department of Chemical Engineering and Biotechnology, University of Cambridge, Philippa Fawcett Drive, Cambridge CB3 0AS, United Kingdom*

SECTION 1. Orientational order parameters $\langle P_2 \rangle_b$ and $\langle P_2 \rangle_s$ of IDTBT and PBTTT

In this section, we reported the values of the orientational order parameters $\langle P_2 \rangle_b$ and $\langle P_2 \rangle_s$ as a function of strain for the two semiconducting polymers. $\langle P_2 \rangle_b$ and $\langle P_2 \rangle_s$ are a measure of the degree of alignment of the polymeric chains to the aromatic backbone and the carbon end-to-end of side chains, respectively.

Table S1 Orientational order parameter computed for the backbone ($\langle P_2 \rangle_b$) and for the side chains ($\langle P_2 \rangle_s$) of the undeformed samples and for *X, Y,* and *Z* uniaxial strains (+ 0.5 % and +1.0 %) for IDTBT crystalline interdigitated (X1-IDTBT, X2-IDTBT) and disordered side chains (X2d-IDTBT) structures. For the amorphous phases (a) only the $\langle P_2 \rangle_b$ is reported. Although IDTBT monomeric unit is made of two lateral chains per side, we only reported the $\langle P_2 \rangle_s$ of one of them because they were almost identical.

		$\langle P_2 \rangle_b$	$\langle P_2 \rangle_s$
X1-IDTBT	0.0 %	+0.9618 ± 0.0001	-0.09 ± 0.02
	+0.5 % (*X*)	+0.9622 ± 0.0001	-0.10 ± 0.01
	+0.5 % (Y)	+0.9633 ± 0.0001	-0.13 ± 0.04
	+0.5 % (Z)	+0.9628 ± 0.0001	-0.10 ± 0.01
	+1.0 % (*X*)	+0.9648 ± 0.0001	-0.16 ± 0.03
	+1.0 % (Y)	+0.9652 ± 0.0001	-0.15 ± 0.05
	+1.0 % (Z)	+0.9667 ± 0.0001	-0.17 ± 0.03
X2-IDTBT	0.0 %	+0.9897 ± 0.0002	-0.10 ± 0.09
	+0.5 % (*X*)	+0.9900 ± 0.0002	-0.11 ± 0.04
	+0.5 % (Y)	+0.9905 ± 0.0002	-0.12 ± 0.03
	+0.5 % (Z)	+0.9910 ± 0.0002	-0.10 ± 0.02
	+1.0 % (*X*)	+0.9920 ± 0.0002	-0.14 ± 0.07
	+1.0 % (Y)	+0.9933 ± 0.0002	-0.14 ± 0.06

	+1.0 % (Z)	+0.9940 ± 0.0002	-0.13 ± 0.04
X2d-IDTBT	0.0 %	+0.9009 ± 0.0017	-0.07 ± 0.40
	+0.5 % (*X*)	+0.9011 ± 0.0018	-0.11 ± 0.40
	+0.5 % (Y)	+0.9016 ± 0.0018	-0.12 ± 0.40
	+0.5 % (Z)	+0.9019 ± 0.0018	-0.10 ± 0.40
	+1.0 % (*X*)	+0.9023 ± 0.0018	-0.14 ± 0.41
	+1.0 % (Y)	+0.9028 ± 0.0018	-0.14 ± 0.41
	+1.0 % (Z)	+0.9035 ± 0.0018	-0.13 ± 0.41
a	0.0 %	+0.0852 ± 0.0111	-
	+0.5 % (*X*)	+0.0992 ± 0.0101	-
	+0.5 % (Y)	+0.1023 ± 0.0177	-
	+0.5 % (Z)	+0.0834 ± 0.0145	-
	+1.0 % (*X*)	+0.0819 ± 0.0191	-
	+1.0 % (Y)	+0.0874 ± 0.0139	-
	+1.0 % (Z)	+0.0765 ± 0.0126	-

Table S2 Orientational order parameter computed for the backbone ($\langle P_2\rangle_b$) and for the side chains ($\langle P_2\rangle_s$) of the undeformed samples and for *X, Y,* and *Z* uniaxial strains (+ 0.5 % and +1.0 %) for PBTTT crystalline interdigitated (X1-PBTTT, X2-PBTTT) and disordered side chains (X2d-PBTTT) structures. For the amorphous phases (a) only the $\langle P_2\rangle_b$ is reported.

		$\langle P_2\rangle_b$	$\langle P_2\rangle_s$
X1-PBTTT	0 %	+0.9949 ± 0.0001	-0.17 ± 0.02
	+0.5 % (*X*)	+0.9947 ± 0.0001	-0.20 ± 0.01
	+0.5 % (Y)	+0.9941 ± 0.0001	-0.22 ± 0.02
	+0.5 % (Z)	+0.9943 ± 0.0001	-0.21 ± 0.05
	+1.0 % (*X*)	+0.9955 ± 0.0001	-0.23 ± 0.05
	+1.0 % (Y)	+0.9957 ± 0.0001	-0.29 ± 0.08
	+1.0 % (Z)	+0.9967 ± 0.0001	-0.26 ± 0.08
X2-PBTTT	0.0 %	+0.9947 ± 0.0001	-0.23 ± 0.02
	+0.5 % (*X*)	+0.9948 ± 0.0001	-0.24 ± 0.02
	+0.5 % (Y)	+0.9950 ± 0.0001	-0.24 ± 0.02
	+0.5 % (Z)	+0.9956 ± 0.0001	-0.23 ± 0.03
	+1.0 % (*X*)	+0.9976 ± 0.0001	-0.26 ± 0.06
	+1.0 % (Y)	+0.9977 ± 0.0001	-0.25 ± 0.05
	+1.0 % (Z)	+0.9987 ± 0.0001	-0.22 ± 0.03
X2d-PBTTT	0.0 %	+0.9625 ± 0.0007	-0.08 ± 0.43
	+0.5 % (*X*)	+0.9644 ± 0.0007	-0.12 ± 0.42
	+0.5 % (Y)	+0.9635 ± 0.0007	-0.11 ± 0.42
	+0.5 % (Z)	+0.9638 ± 0.0007	-0.10 ± 0.42
	+1.0 % (*X*)	+0.9655 ± 0.0008	-0.15 ± 0.41
	+1.0 % (Y)	+0.9656 ± 0.0008	-0.14 ± 0.42
	+1.0 % (Z)	+0.9677 ± 0.0007	-0.14 ± 0.41
a	0.0 %	+0.1050 ± 0.0100	-
	+0.5 % (*X*)	+0.1123 ± 0.0155	-
	+0.5 % (Y)	+0.1187 ± 0.0127	-
	+0.5 % (Z)	+0.1345 ± 0.0175	-
	+1.0 % (*X*)	+0.1198 ± 0.0159	-
	+1.0 % (Y)	+0.0956 ± 0.0185	-
	+1.0 % (Z)	+0.1139 ± 0.0135	-

SECTION 2. Dihedral distributions and deviation from planarity of IDTBT and PBTTT

The following section reports the dihedral distribution of the crystalline and amorphous phases of both IDTBT and PBTTT polymers. Dihedral distributions are reported at the undeformed stage (orange plot of Figures 1-3) and after the application of two positive applied strains (+0.5% and +1.0% corresponding to the purple and green plots, respectively of Figure S1-S3). Three different plots are reported according to the direction of application of the uniaxial strain, namely along the *X*, *Y,* and *Z* axes. By comparing the torsional angle profiles for the X1- X2- and the X2d- phases of IDTBT and PBTTT, very few variations in the dihedral profile can be attributed to the application of uniaxial strains. However, notable differences can be found between the interdigitated and non-interdigitated structures. Indeed, in the case of interdigitated X2d-PBTTT the perfect registry of the side chains leads to a planar polymer backbone, while for X2d-PBTTT a decrease in backbone planarity is accompanied by a higher π −overlap between the dithiophene units. Regarding the amorphous phases, the small displacements induced by the strain did not significantly affect the dihedral profiles.

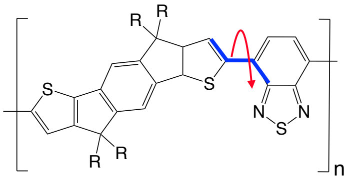

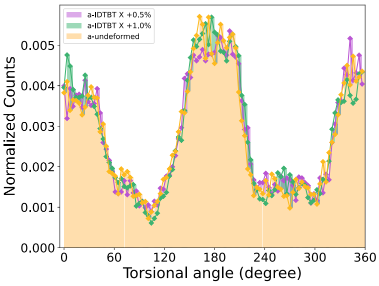

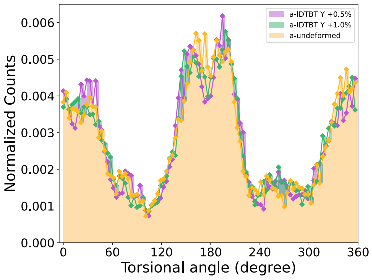

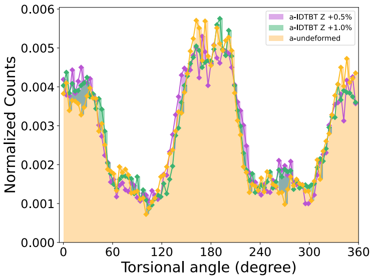

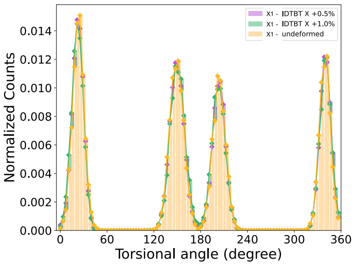

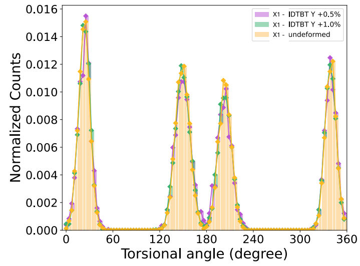

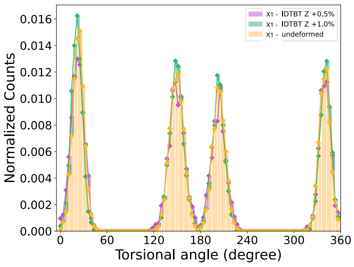

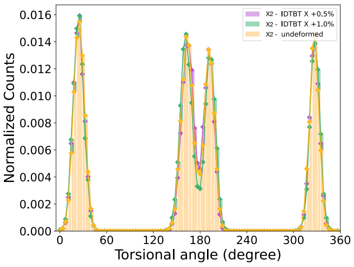

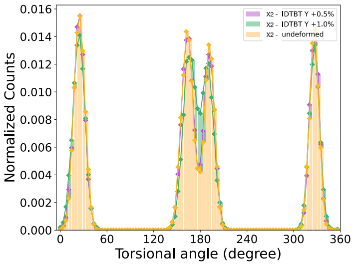

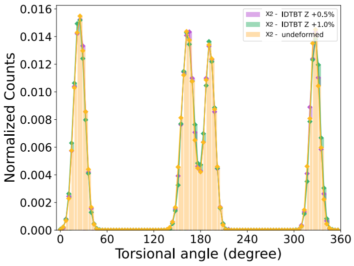

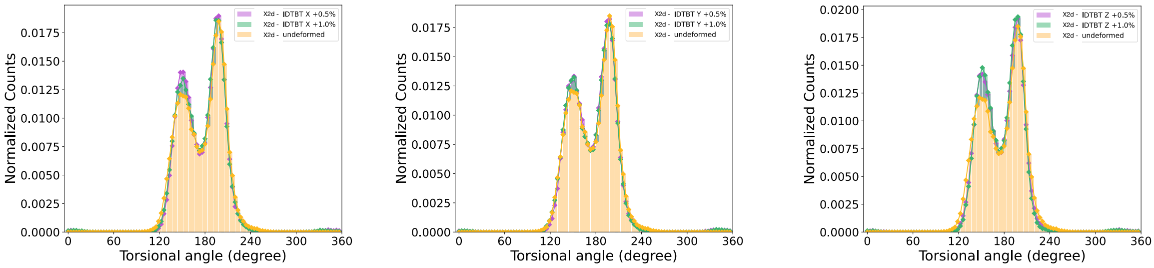

Figure S1 a-IDTBT (first row), X1-IDTBT (second row), X2-IDTBT (third row), X2d-IDTBT (fourth row) torsional profiles for the undeformed (orange) and deformed ones (+0.5 % (purple) and +1.0 % (green)). Strain is applied along the *X* (first column), *Y* (second column), and *Z* (third column) axes. The sketch of the torsional angle is reported at the top of the panel.

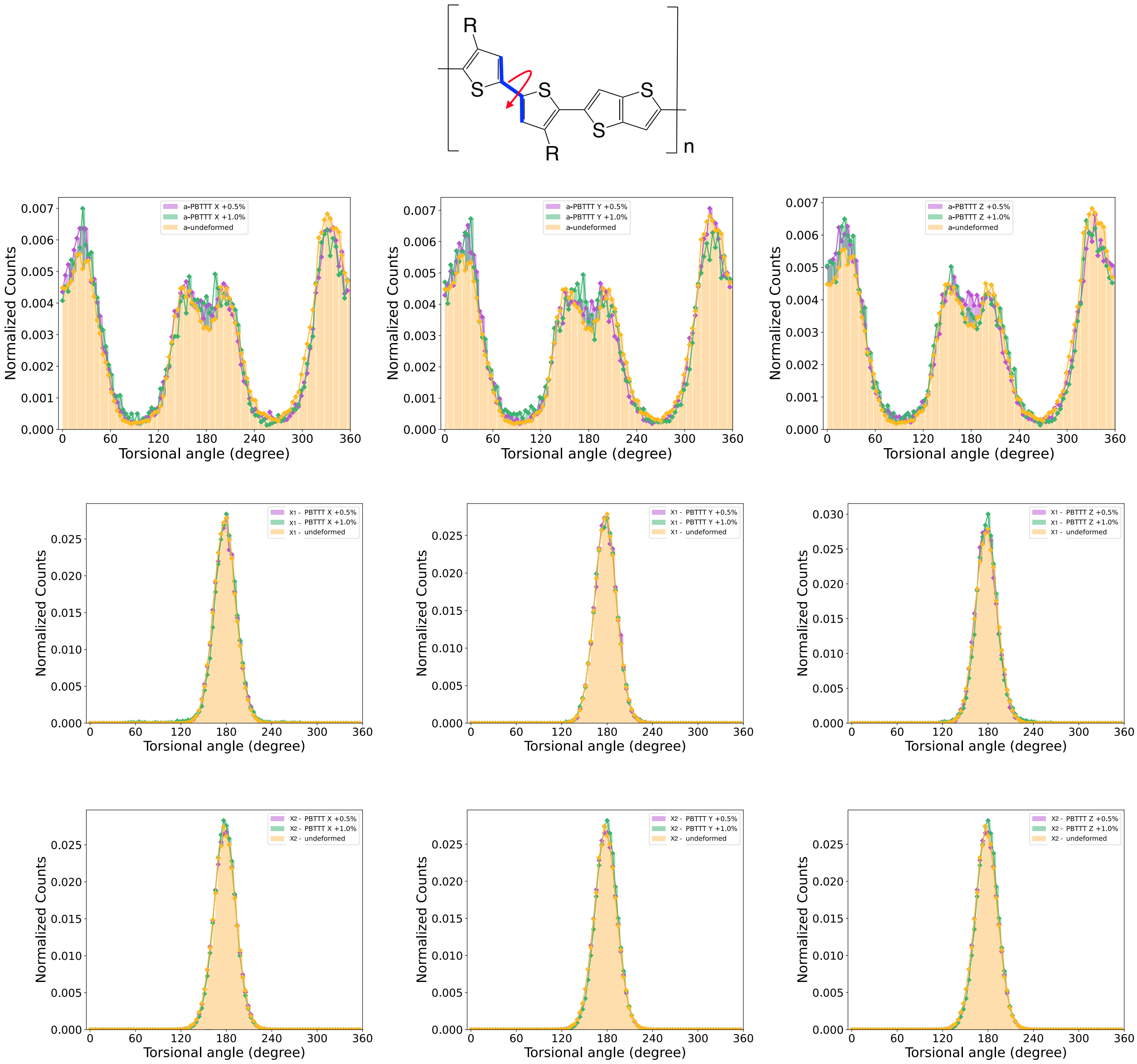

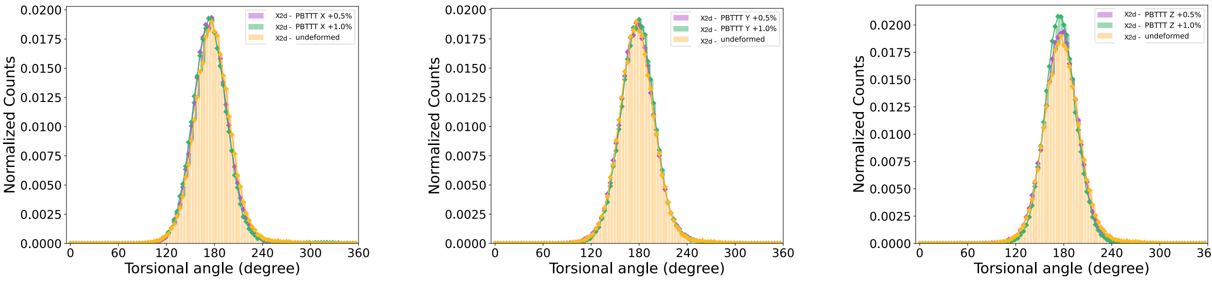

Figure S2 a-PBTTT (first row), X1-PBTTT (second row), X2-PBTTT (third row), X2d-PBTTT (fourth row) torsional profiles (inter-monomer) for the undeformed (orange) and deformed ones (+0.5 % (purple) and +1.0 % (green)). Strain is applied along the *X* (first column), *Y* (second column), and *Z* (third column) axes. The sketch of the torsional angle is reported at the top of the panel.

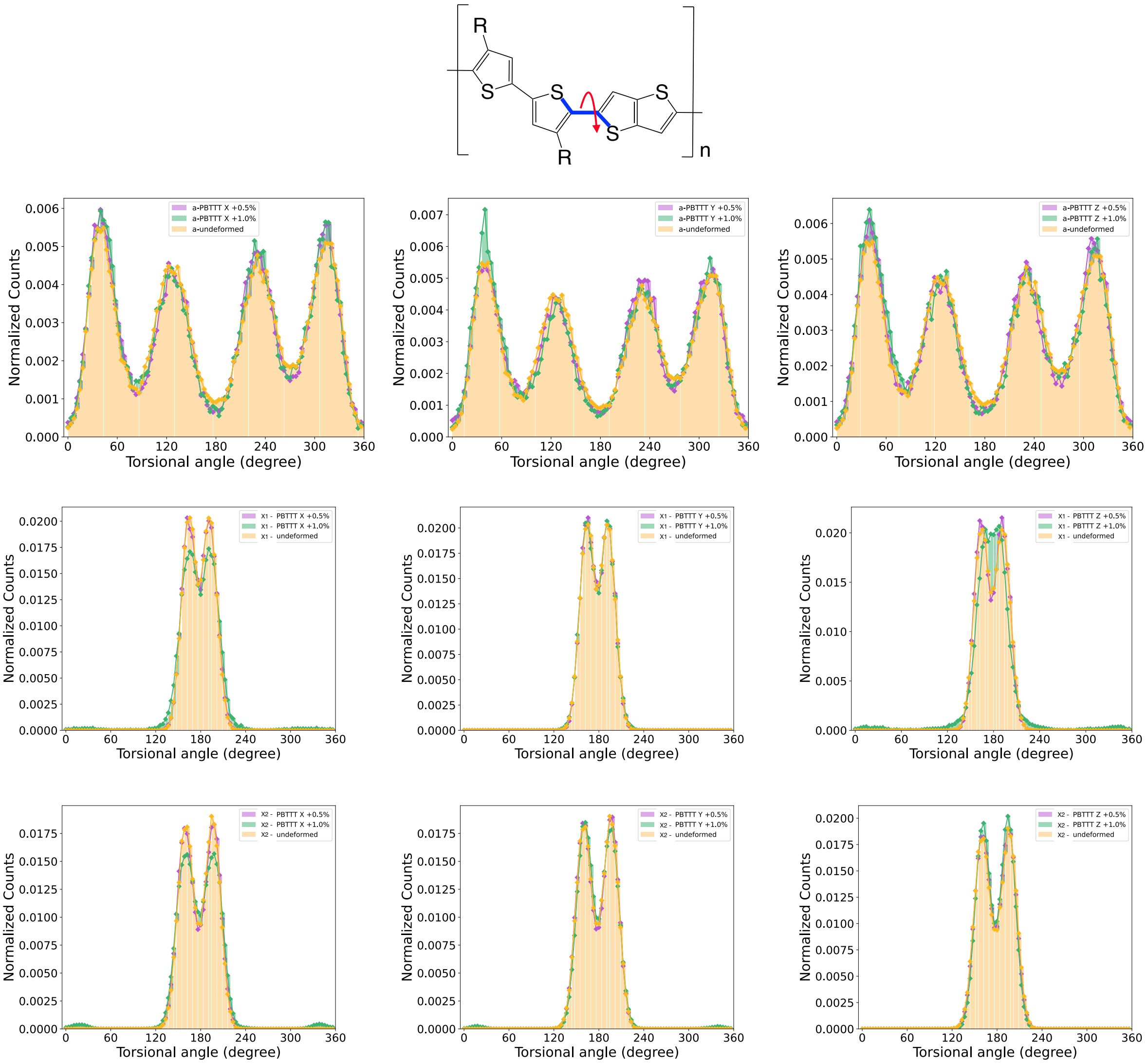

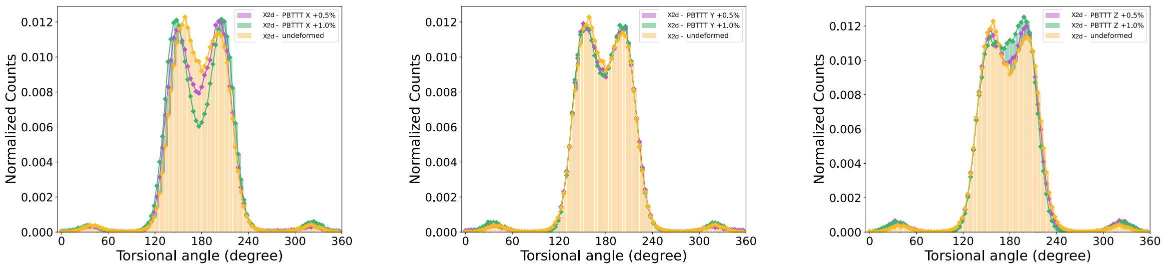

Figure S3 a-PBTTT (first row), X1-PBTTT (second row), X2-PBTTT (third row), X2d-PBTTT (fourth row) torsional profiles (intra-monomer) for the undeformed (orange) and deformed ones (+0.5 % (purple) and +1.0 % (green)). Strain is applied along the *X* (first column), *Y* (second column), and *Z* (third column) axes. The sketch of the torsional angle is reported at the top of the panel.

Additional structural insights on the effects of the applied strain were obtained by quantifying the deviation from planarity of the aromatic backbone in PBTTT and IDTBT. This deviation was analyzed as a function of increasing positional order, transitioning from the amorphous to the crystalline phases. Deviations from planarity were averaged over torsional angle distributions computed from equilibrated NVT simulation. Exploiting the monomer symmetry, torsional angles were converted in the 0°-90° range.

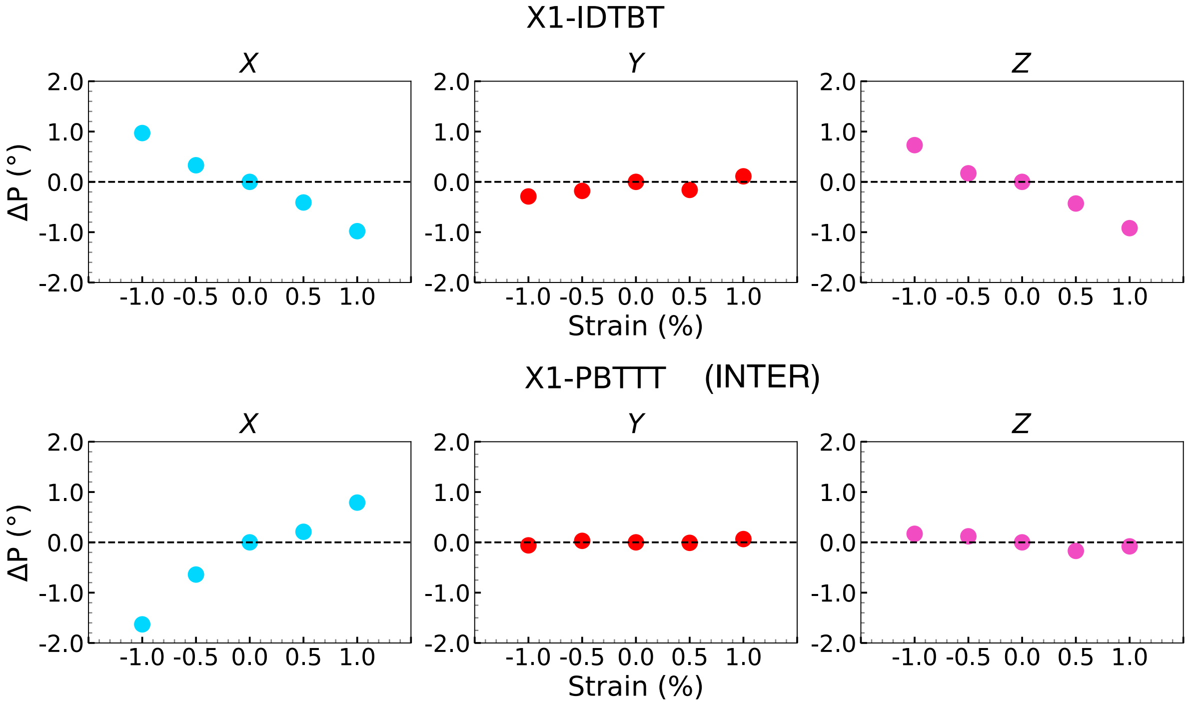

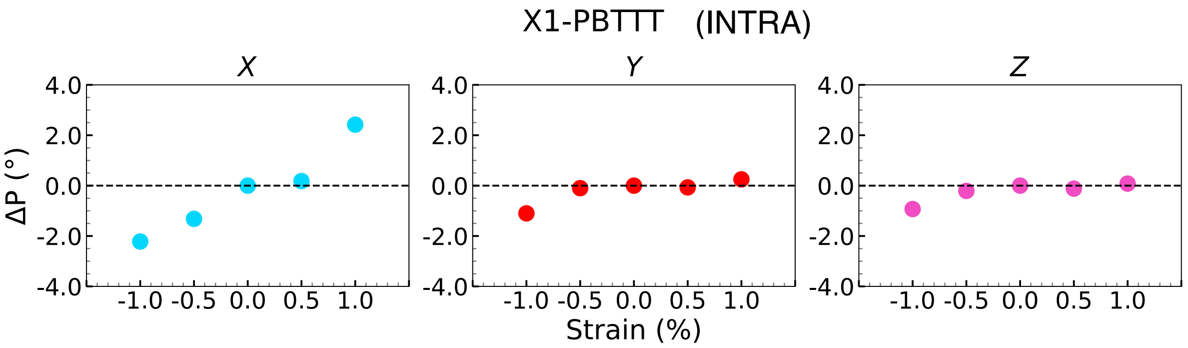

Figure S4 X1-IDTBTT (top), X1-PBTTT inter-monomer dihedral (center) and X1-PBTTT intra-monomer (bottom) deviation of planarity ΔP (computed as ΔP = P(ε_0) - P(ε), where ε_0 is the absence of strain) as a function of strain along the *X, Y* and *Z* axes.

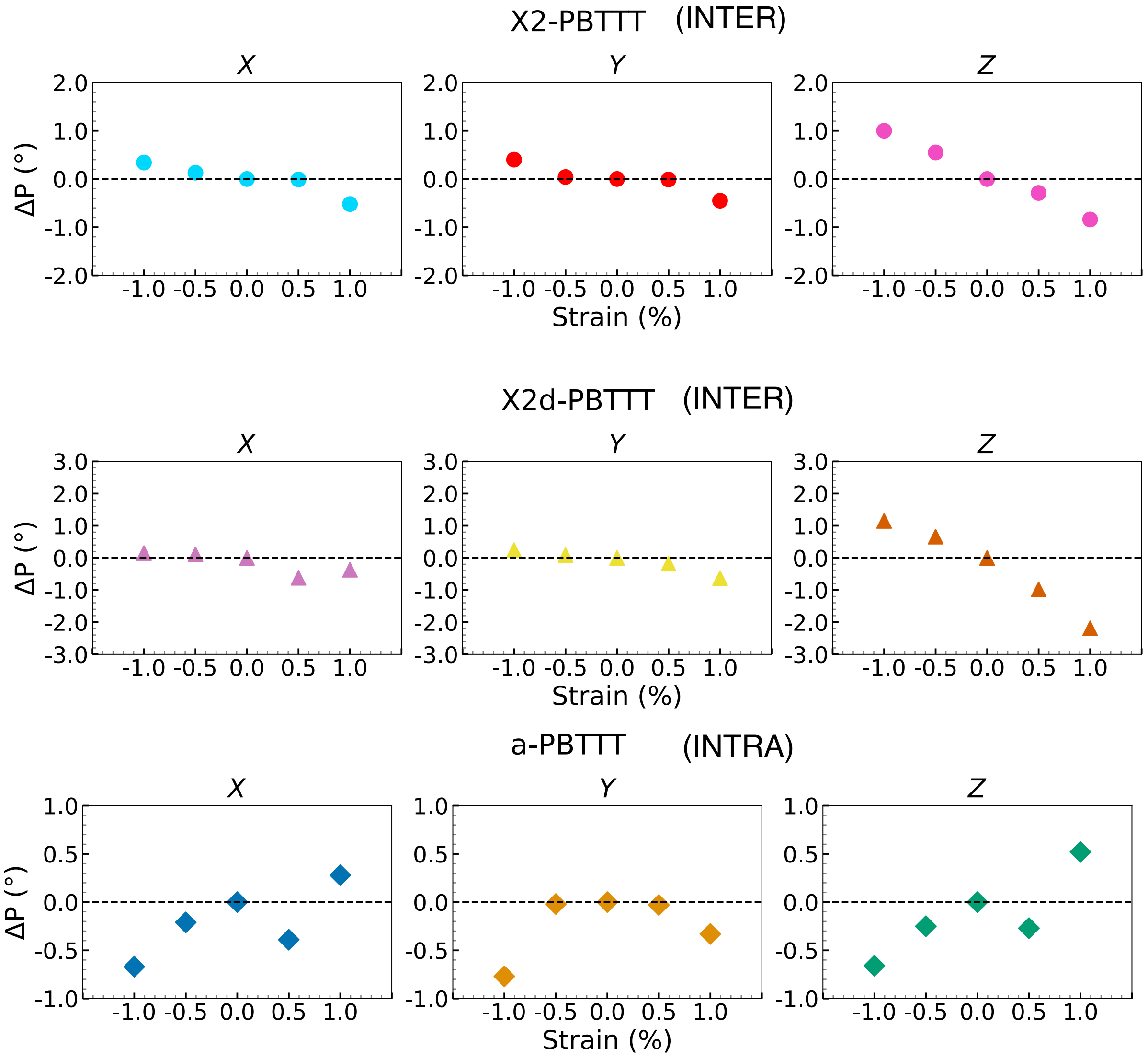

Figure S5 X2-PBTTT inter-monomer dihedral (top), X2d-PBTTT inter-monomer (center) and a-PBTTT intra-monomer (bottom) deviation of planarity ΔP (computed as ΔP = P(ε_0) - P(ε), where ε_0 is the absence of strain) as a function of strain along the *X, Y* and *Z* axes.

Table S3 X1-, X2-, X2d, and a-IDTBT average backbone deviation from planarity and its standard deviation as a function of strain along the *X, Y* and *Z* axes.

	Deviation from planarity (°)		
		X1-IDTBT	
0%		24.8 ± 8.7	
	X	*Y*	*Z*
-1.0%	25.8 ± 8.5	24.5 ± 8.7	25.5 ± 8.9
-0.5%	25.1 ± 8.7	24.6 ± 8.7	25.0 ± 8.9
+0.5%	24.4 ± 8.8	24.6 ± 9.4	24.4 ± 8.6
+1.0%	23.8 ± 8.9	24.9 ± 8.9	23.9 ± 8.7
		X2-IDTBT	
0%		21.6 ± 10.0	
	X	*Y*	*Z*
-1.0%	22.0 ± 9.8	21.9 ± 9.6	22.0 ± 10.0
-0.5%	21.7 ± 9.9	21.6 ± 9.9	21.6 ± 10.0
+0.5%	21.2 ± 10.1	21.3 ± 10.0	21.4 ± 10.0
+1.0%	21.2 ± 9.4	21.3 ± 11.0	21.1 ± 9.9
		X2d-IDTBT	
0%		23.8 ± 13.6	
	X	*Y*	*Z*
-1.0%	24.1 ± 12.5	24.3 ± 12.3	25.0 ± 12.5
-0.5%	24.0 ± 12.9	24.0 ± 12.8	24.7 ± 12.0
+0.5%	22.5 ± 12.4	23.2 ± 12.9	22.1 ± 12.1
+1.0%	22.4 ± 12.6	22.8 ± 12.2	21.5 ± 11.7
		a-IDTBT	
0%		33.1 ± 23.9	
	X	*Y*	*Z*
-1.0%	33.6 ± 24.1	32.7 ± 23.9	32.7 ± 23.7
-0.5%	33.3 ± 24.1	33.1 ± 23.8	33.5 ± 23.7
+0.5%	33.3 ± 23.9	33.6 ± 23.8	33.8 ± 24.0
+1.0%	32.6 ± 23.9	33.7 ± 23.8	33.9 ± 24.3

Table S4 X1-, X2-, X2d, and a-PBTTT intra-monomer and inter-monomer average backbone deviation from planarity and its standard deviation as a function of strain along the *X, Y* and *Z* axes.

Deviation from planarity (°)							
		X1-PBTTT (INTER)				**X1-PBTTT (INTRA)**	
0%		11.7 ± 8.9		0%		15.0 ± 8.9	
	X	*Y*	*Z*		*X*	*Y*	*Z*
-1.0%	10.0 ± 8.0	11.5 ± 9.1	11.8 ± 10.1	-1.0%	12.8 ± 10.6	13.9 ± 9.0	14.1 ± 10.3
-0.5%	11.0 ± 8.3	11.7 ± 9.0	11.7 ± 9.0	-0.5%	13.7 ± 9.0	14.9 ± 9.1	14.8 ± 9.0
+0.5%	11.9 ± 9.1	11.6 ± 8.9	11.4 ± 8.8	+0.5%	15.2 ± 9.0	14.9 ± 8.8	14.9 ± 8.6
+1.0%	12.5 ± 11.2	11.8 ± 9.0	11.5 ± 9.9	+1.0%	17.4 ± 11.7	15.2 ± 9.1	15.1 ± 10.6
		X2-PBTTT (INTER)				**X2-PBTTT (INTRA)**	
0%		12.0 ± 9.3		0%		18.4 ± 10.0	
	X	*Y*	*Z*		*X*	*Y*	*Z*
-1.0%	12.3 ± 9.0	12.4 ± 9.1	13.0 ± 9.1	-1.0%	17.6 ± 11.1	18.9 ± 10.0	19.2 ± 10.0
-0.5%	12.1 ± 9.1	12.0 ± 9.1	12.5 ± 9.0	-0.5%	18.0 ± 10.7	18.6 ± 9.9	19.0 ± 9.7
+0.5%	12.0 ± 9.2	12.0 ± 9.1	11.7 ± 9.0	+0.5%	18.9 ± 10.1	18.6 ± 9.9	18.0 ± 9.8
+1.0%	11.5 ± 8.9	11.5 ± 8.9	11.2 ± 8.5	+1.0%	19.4 ± 11.2	18.1 ± 10.0	17.3 ± 9.4
		X2d-PBTTT (INTER)				**X2d-PBTTT (INTRA)**	
0%		17.8 ± 14.5		0%		24.5 ± 15.0	
	X	*Y*	*Z*		*X*	*Y*	*Z*
-1.0%	18.0 ± 13.9	18.1 ± 15.0	19.0 ± 13.1	-1.0%	22.9 ± 15.1	24.1 ± 14.9	25.9 ± 14.8
-0.5%	18.0 ± 14.1	18.0 ± 14.9	18.5 ± 13.8	-0.5%	23.1 ± 14.8	24.7 ± 15.0	24.8 ± 14.9
+0.5%	17.3 ± 13.3	17.7 ± 14.2	16.9 ± 13.4	+0.5%	26.1 ± 15.2	24.7 ± 14.8	23.8 ± 14.4
+1.0%	17.5 ± 13.8	17.2 ± 13.7	15.7 ± 12.2	+1.0%	28.2 ± 15.0	24.7 ± 14.6	22.7 ± 14.0
		a-PBTTT (INTER)				**a-PBTTT (INTRA)**	
0%		28.9 ± 18.2		0%		48.7 ± 19.9	
	X	*Y*	*Z*		*X*	*Y*	*Z*
-1.0%	28.2 ± 18.4	29.0 ± 18.2	29.0 ± 18.2	-1.0%	48.0 ± 20.0	47.9 ± 19.3	48.0 ± 19.7
-0.5%	28.2 ± 18.2	28.1 ± 18.3	28.5 ± 18.3	-0.5%	48.5 ± 19.6	48.6 ± 19.6	48.4 ± 19.4
+0.5%	28.3 ± 18.1	28.5 ± 18.3	28.2 ± 18.5	+0.5%	48.3 ± 19.3	48.3 ± 19.7	48.4 ± 19.4
+1.0%	28.8 ± 16.6	28.8 ± 18.8	28.9 ± 18.4	+1.0%	48.9 ± 19.3	48.3 ± 19.5	49.2 ± 19.5

SECTION 3. Pressure tensor of the amorphous, crystalline and non-interdigitated phases of IDTBT and PBTTT

We reported in Table S1 the average values of the six independent components of the pressure tensor $\langle \boldsymbol{P} \rangle$ for the investigated phases, namely the amorphous (a), interdigitated crystalline (X1-, X2-), and disordered side chains (X2d-) phases. In the case of the amorphous sample, the isotropic pressure value of a-IDTBT differs from atmospheric pressure, although we ensured that cell box dimensions had reached convergency in the former NPT equilibration trajectory. For the more ordered phases we measured an isotropic pressure close to 1 bar for all conformers, except for the X2d-IDTBT, which we found to be equilibrated at -79 bar. Generally, we detected a decrease in $\langle \boldsymbol{P} \rangle$ for the non-interdigitated structures compared to the corresponding interdigitated ones. We address this behavior to the lower degree of packing since alkyl side chains are farther apart and thus, to a decrease in density computed from the simulation, namely from 1.9 to 0.9 g/mL for the interdigitated and non-interdigitated phases, respectively.

Table S5 IDTBT and PBTTT averaged pressure tensor components of the undeformed samples for the amorphous (a), crystalline interdigitated (I) and non-interdigitated (NI) phases calculated along equilibrated NVT trajectories at T=298 K. The total average pressure ($\langle P \rangle$) is calculated as $P = (tr\ \langle \boldsymbol{P} \rangle)/3$.

	$\langle P_{XX} \rangle$ (bar)	$\langle P_{XY} \rangle$ (bar)	$\langle P_{XZ} \rangle$ (bar)	$\langle P_{YY} \rangle$ (bar)	$\langle P_{YZ} \rangle$ (bar)	$\langle P_{ZZ} \rangle$ (bar)	$\langle P \rangle$ (bar)
a-IDTBT	30	24	47	63	-47	20	38
a-PBTTT	6	-40	-40	21	89	-28	0
X1-IDTBT	4371	3794	-2768	-1932	1502	-2476	12
X2-IDTBT	-256	30	-88	199	-91	-181	79
X2d-IDTBT	-106	1082	602	-168	829	176	32
X1-PBTTT	131	3279	-2014	20	-5869	-123	9
X2-PBTTT	0.3	1117	818	6	-1978	2	-3
X2d-PBTTT	-123	-57	107	193	75	-72	30

SECTION 4. Stiffness tensor ($\boldsymbol{C}$) and of IDTBT and PBTTT

The complete stiffness tensor ($\boldsymbol{C_{FIT}}$), a 3x3 matrix, was calculated for the amorphous and the crystalline phases as according to the fitting procedure described in the main paper. Values are reported in Table S5.

Table S6 $\boldsymbol{C_{FIT}}$ components calculated for IDTBT and PBTTT amorphous (a), crystalline interdigitated (I) and non-interdigitated (NI) phases. Due to the internal symmetry of the amorphous samples, we reported in the table only the two independent terms that define the stiffness tensor.

	C_{11} (GPa)	C_{12} (GPa)	C_{13} (GPa)	C_{22} (GPa)	C_{23} (GPa)	C_{33} (GPa)
a-IDTBT	4.0	3.2	-	-	-	-
a-PBTTT	4.2	3.1	-	-	-	-
X1-IDTBT	18.2	11.3	13.6	13.6	13.0	60.2
X2-IDTBT	17.9	9.2	5.1	33.5	14.8	42.0
X2d-IDTBT	19.5	5.2	6.4	27.0	11.3	38.2
X1-PBTTT	10.8	8.9	15.7	16.2	11.2	90.9
X2-PBTTT	16.3	10.9	11.8	10.8	15.7	102.3
X2d-PBTTT	18.9	7.9	9.8	16.9	18.7	100.4

SECTION 5. Poisson's ratio of the interdigitated and non-interdigitated phases of IDTBT and PBTTT

In order to compute the Poisson's ratio (reported in Table S3) of the crystalline interdigitated and the non-interdigitated phases we determined the compliance tensor ($\boldsymbol{S_{FIT}}$) from the stiffness tensor ($\boldsymbol{C_{FIT}}$) as $\boldsymbol{S_{FIT}} = \boldsymbol{C_{FIT}^{-1}}$. We derived both Young's modulus and Poisson's ratio directly from $\boldsymbol{S_{FIT}}$ as follows [1]:

$$\begin{aligned} E_X &= 1/S_{XX} \\ E_Y &= 1/S_{YY} \\ E_Z &= 1/S_{ZZ} \\ \nu_{XY} &= -S_{XX}/E_Y \\ \nu_{XZ} &= -S_{XZ}/E_Z \\ \nu_{YX} &= -S_{YX}/E_X \\ \nu_{YZ} &= -S_{YZ}/E_Z \\ \nu_{ZX} &= -S_{ZX}/E_X \\ \nu_{ZY} &= -S_{ZY}/E_Y \end{aligned} \qquad \text{(SE1)}$$

Table S7 Poisson's ratios ($\nu_{\alpha\beta}$) for IDTBT and PBTT crystalline interdigitated (I) and non-interdigitated (NI) phases computed from *NVT* equilibrated simulations at *T*=298 K.

	ν_{XY}	ν_{XZ}	ν_{YX}	ν_{YZ}	ν_{ZX}	ν_{ZY}
X1-IDTBT	0.43	0.07	0.26	0.42	0.02	0.30
X2-IDTBT	0.55	0.32	0.67	0.58	0.06	0.09
X2d-IDTBT	0.44	0.52	0.57	0.53	0.10	0.11
X1-PBTTT	0.10	0.43	0.08	0.28	0.37	0.04
X2-PBTTT	0.12	0.53	0.07	0.39	0.52	0.06
X2d-PBTTT	0.22	0.47	0.10	0.33	0.40	0.20

SECTION 6. Energy contributions vs strain for IDTBT and PBTTT

Figures S6-8 are representative of the total, bonded and non-bonded energy contributions of the amorphous (a-IDTBT/PBTTT) and crystalline (X2d-, X2, X1-IDTBT/PBTTT) phases as a function of strain in the range -1.0 % to +1.0% with a step of 0.5%. Energy values, corresponding to the dots in the plots, are computed as the average over equilibrated NVT trajectories. Continuous lines correspond to the attempt to fit the parabolic trend.

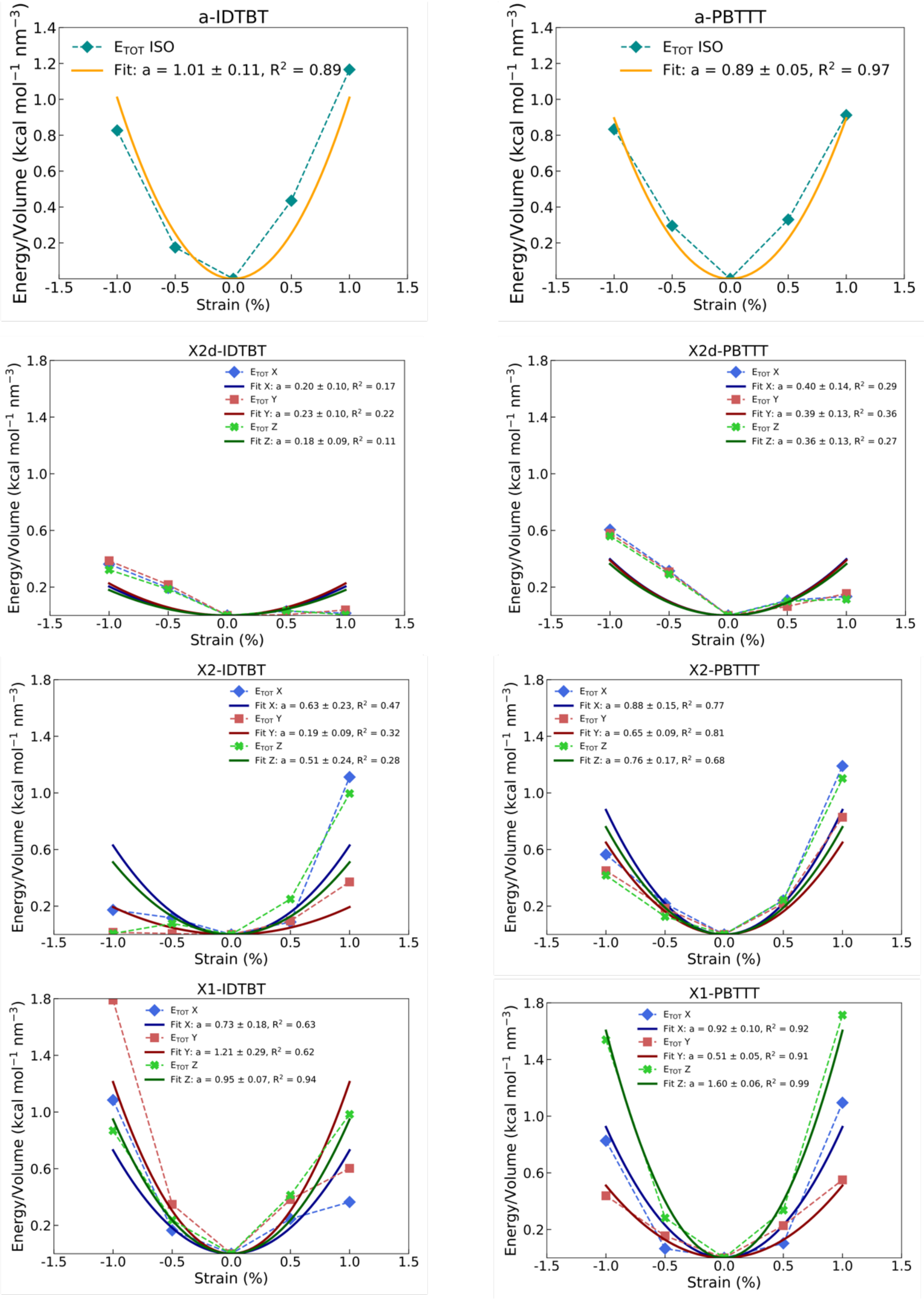

Figure S6 Total energy contributions from bonded and non-bonded terms ($E_{TOT} = E_{BONDED} + E_{NON\text{-}BONDED}$) as a function of strain. For the amorphous phases a-IDTBT and a-PBTTT, we herein show only the isotropic strain, *i.e.* the average over the *X, Y,* and *Z* uniaxial strains. In the case of the highly crystalline (X1-IDTBT/PBTTT and X2-IDTBT/PBTTT) and the more disordered crystalline (X2d-IDTBT/PBTTT) phases, we differentiated between the three directions of applied strain along the *X, Y,* and *Z* axes. The points in the plots correspond to the average values we obtained from the MD simulations, and the dotted lines are just guides for the eyes. Continuous lines represent our attempt to fit the parabolic trend of the energy versus strain ($y=ax^2$). Legends in the plots state the value of a along with its standard deviation and the parameter R², which represents the goodness of fit.

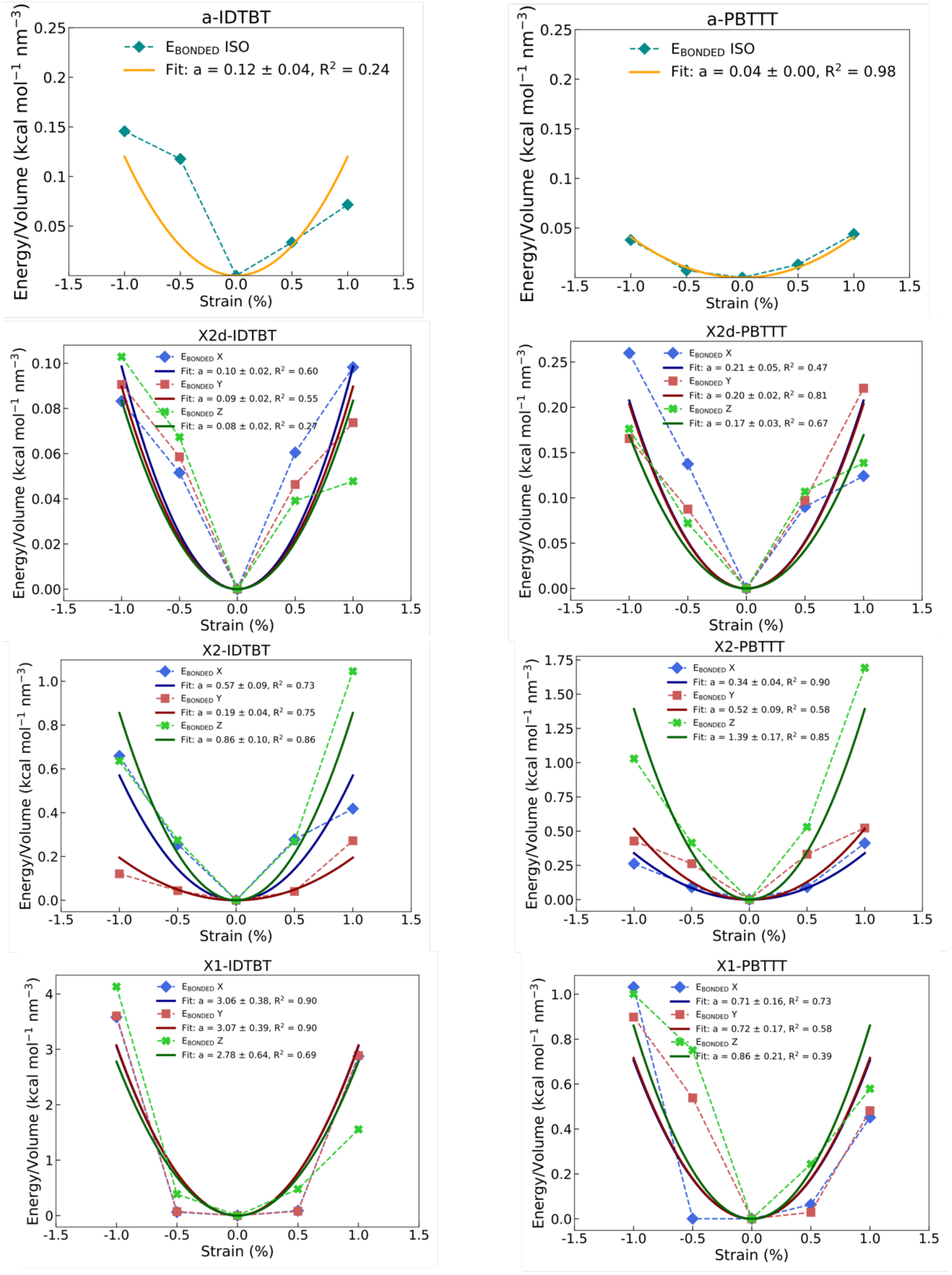

Figure S7 Bonded energy, E_{BONDED}, as a function of strain. For the amorphous phases a-IDTBT and a-PBTTT, we herein show only the isotropic strain, *i.e.* the average over the *X, Y,* and *Z* uniaxial strains. In the case of the highly crystalline (X1-IDTBT/PBTTT and X2-IDTBT/PBTTT) and the more disordered crystalline (X2d-IDTBT/PBTTT) phases, we differentiated between the three directions of applied strain along the *X, Y,* and *Z* axes. The points in the plots correspond to the average values we obtained from the MD simulations, and the dotted lines are just guides for the eyes. Continuous lines represent our attempt to fit the parabolic trend of the energy versus strain ($y=ax^2$). Legends in the plots state the value of a along with its standard deviation and the parameter R^2, which represents the goodness of fit.

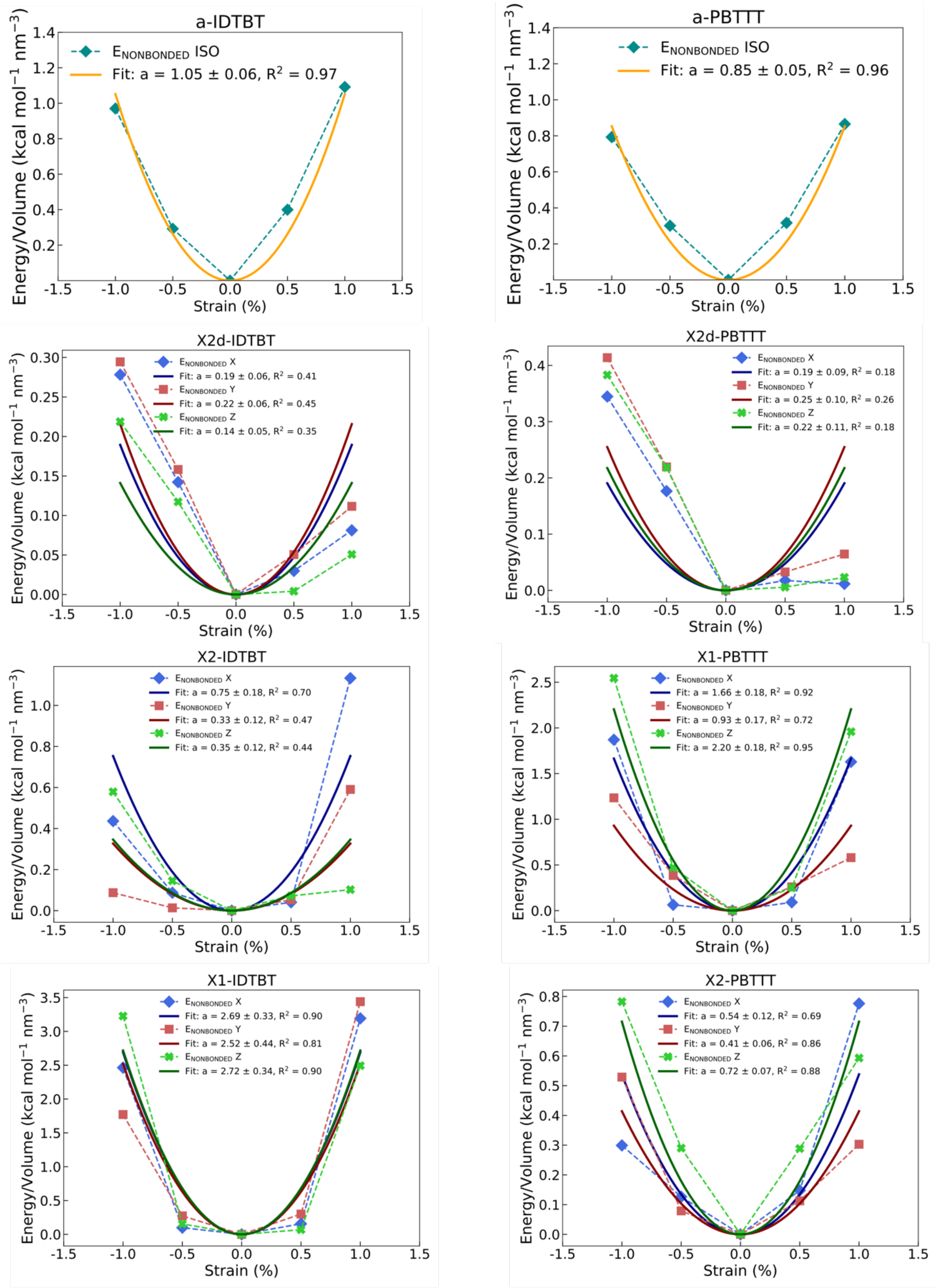

Figure S8 Non-bonded energy contributions, $E_{\text{NON-BONDED}}$, as a function of strain. For the amorphous phases a-IDTBT and a-PBTTT, we herein show only the isotropic strain, *i.e.* the average over the *X, Y,* and *Z* uniaxial strains. In the case of the highly crystalline (X1-IDTBT/PBTTT and X2-IDTBT/PBTTT) and the more disordered crystalline (X2d-IDTBT/PBTTT) phases, we differentiated between the three directions of applied strain along the *X, Y,* and *Z* axes. The points in the plots correspond to the average values we obtained from the MD simulations, and the dotted lines are just guides for the eyes. Continuous lines represent our attempt to fit the parabolic trend of the energy versus strain ($y=ax^2$). Legends in the plots state the value of a along with its standard deviation and the parameter R^2, which represents the goodness of fit.

SECTION 7. Radial distribution functions (g(r)) for IDTBT and PBTTT

Radial distribution functions, g(r) are computed with respect to the sulfur atoms inside the monomeric units as the average over equilibrated NVT simulations for the amorphous (a-IDTBT/PBTTT) and crystalline (X2d-, X2, X1-IDTBT/PBTTT) samples.

IDTBT

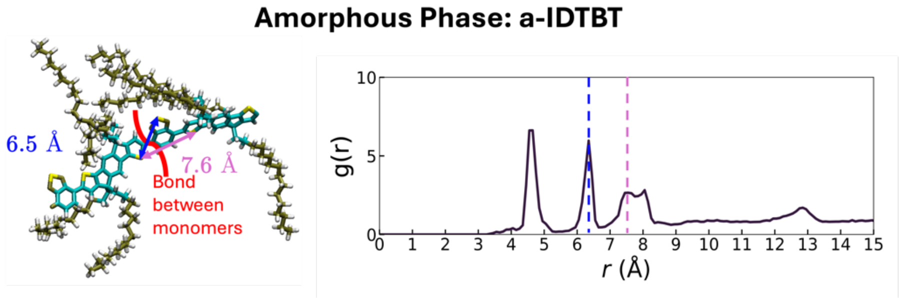
Amorphous Phase: a-IDTBT

Figure S9 Radial distribution function g(r) of a-IDTBT with the assignment of inter-chain peaks.

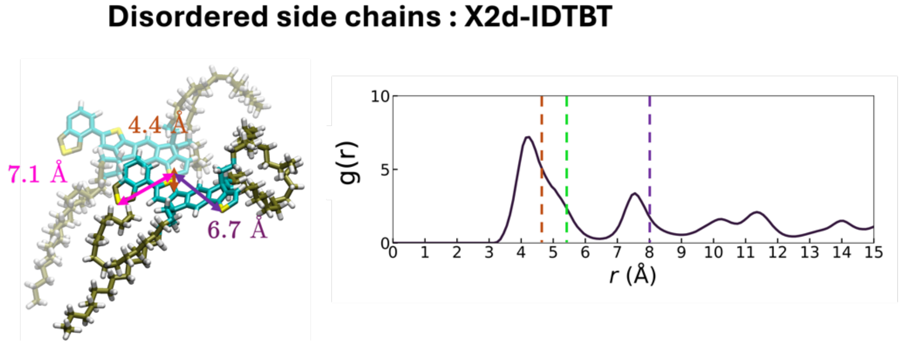
Disordered side chains : X2d-IDTBT

Figure S10 Radial distribution function g(r) of X2d-IDTBT with the assignment of inter-chain peaks.

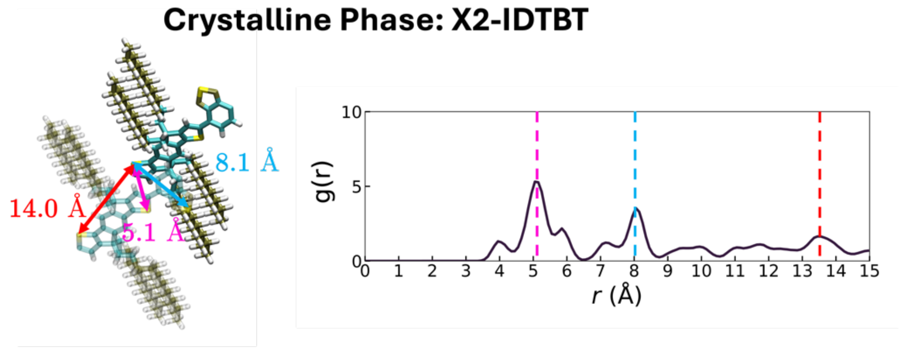
Crystalline Phase: X2-IDTBT

Figure S11 Radial distribution function g(r) of X2-IDTBT with the assignment of inter-chain peaks.

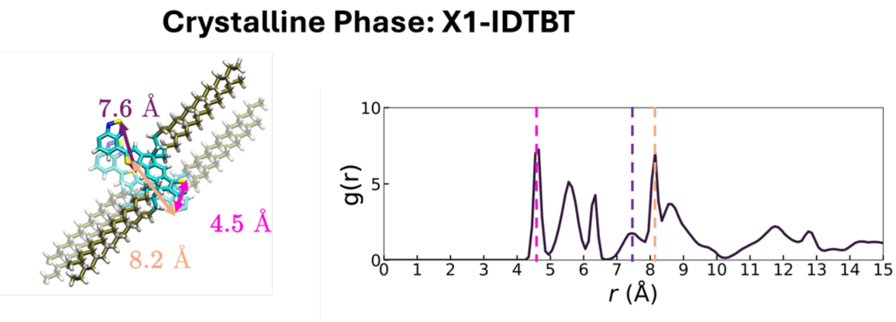

Figure S12 Radial distribution function g(r) of X1-IDTBT with the assignment of inter-chain peaks.

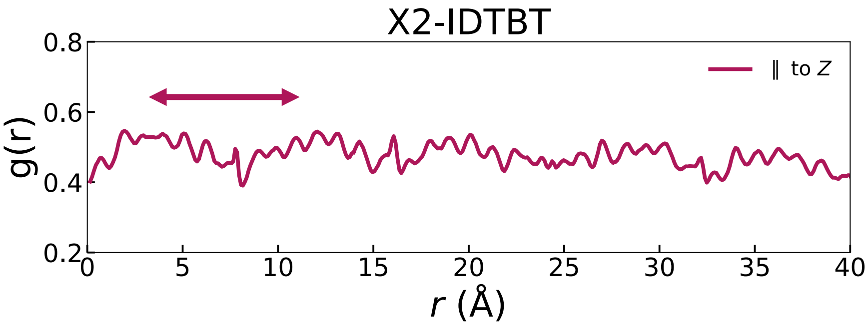

Figure S13 Radial distribution function g(r) of X2-IDTBT computed parallel to the backbone axis. The arrow highlights the periodic peaks corresponding to monomer lengths along the polymeric chain.

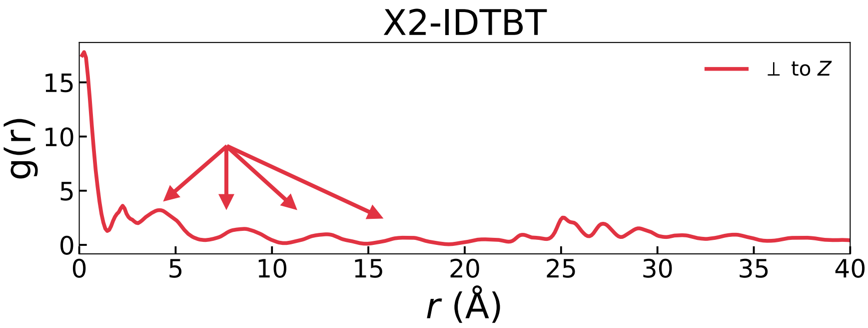

Figure S14 Radial distribution function g(r) of X2-IDTBT computed perpendicular to the backbone axis. Arrows point to the periodic peaks corresponding to π-stacking interaction among polymeric chains. The broad peaks above 25 Å correspond to the interlamellar planes.

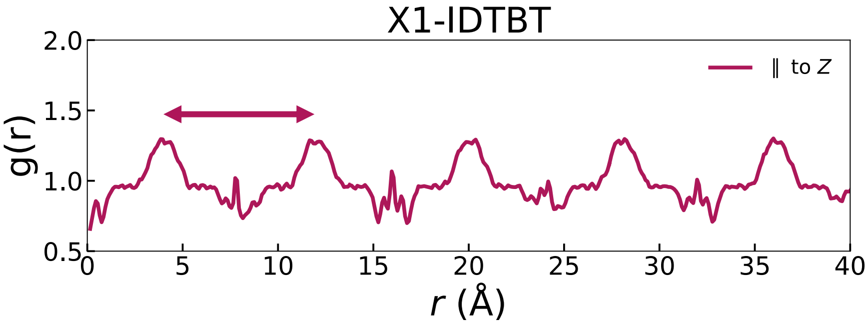

Figure S15 Radial distribution function (RDF) of X1-IDTBT computed parallel to the backbone axis. The arrow highlights the periodic peaks corresponding to monomer lengths along the polymeric chain.

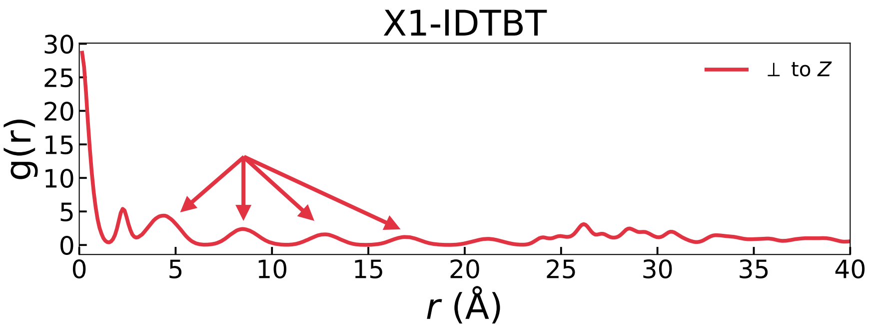

Figure S16 Radial distribution function (RDF) of X1-IDTBT computed perpendicular to the backbone axis. Arrows point to the periodic peaks corresponding to π-stacking interaction among polymeric chains. The broad peaks above 25 Å correspond to the interlamellar planes.

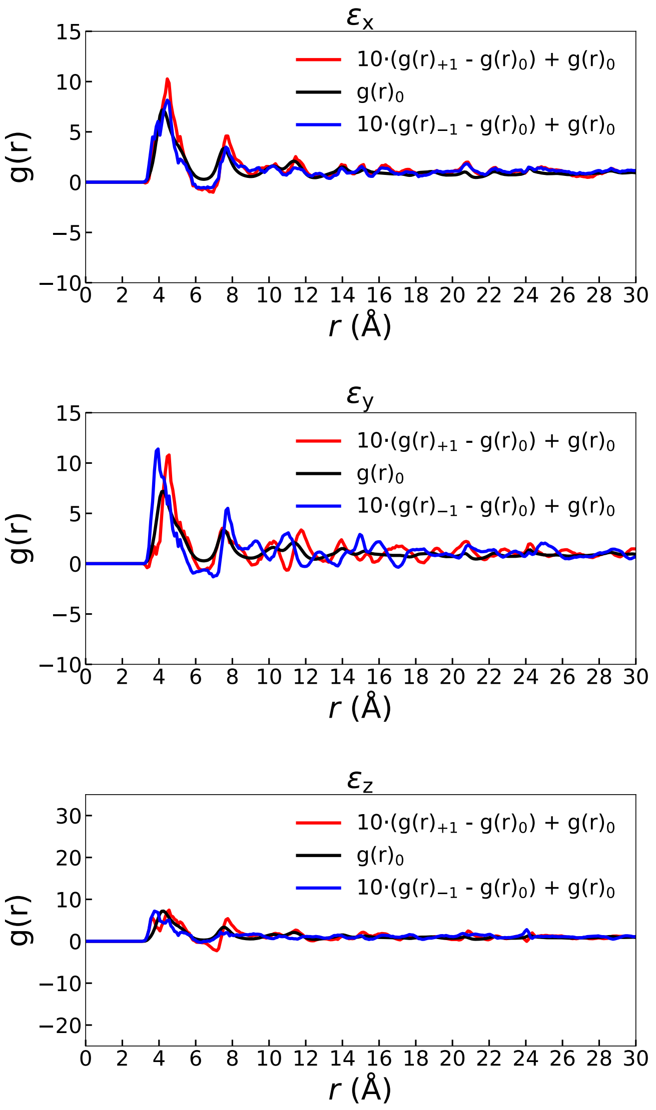

Figure S17 Radial distribution function, g(r), of X2d-IDTBT for ε=0%, ε=+1.0% and ε=-1.0% along the *X, Y* and *Z* axes. To highlight changes, in each plot is shown the g(r)$_0$ (black line) for ε=0%, and 10(g(r)$_{\pm1}$ g(r)$_0$)+ g(r)$_0$ for ε=+1.0% and ε=-1.0% (red and blue lines for ε=-1.0% and ε=+1.0%, respectively).

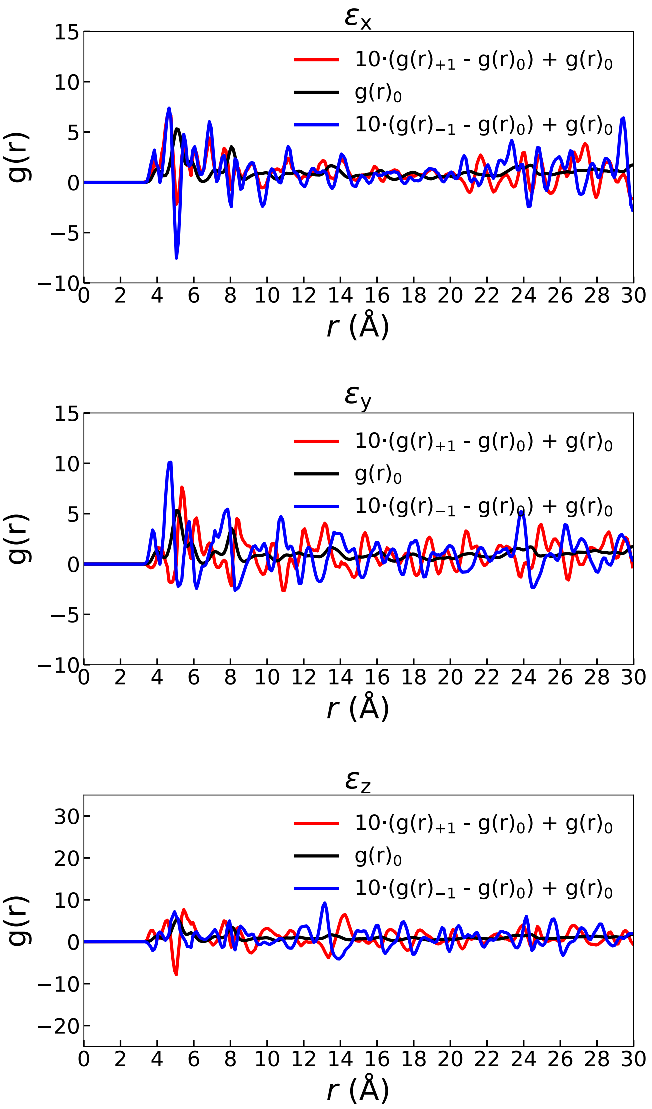

Figure S18 Radial distribution function, g(r), of X2-IDTBT for ε=0%, ε=+1.0% and ε=-1.0% along the *X, Y* and *Z* axes. To highlight changes, in each plot is shown the $g(r)_0$ (black line) for ε=0%, and 10($g(r)_{\pm 1}$ $g(r)_0$)+ $g(r)_0$ for ε=+1.0% and ε=-1.0% (red and blue lines for ε=-1.0% and ε=+1.0%, respectively).

PBTTT

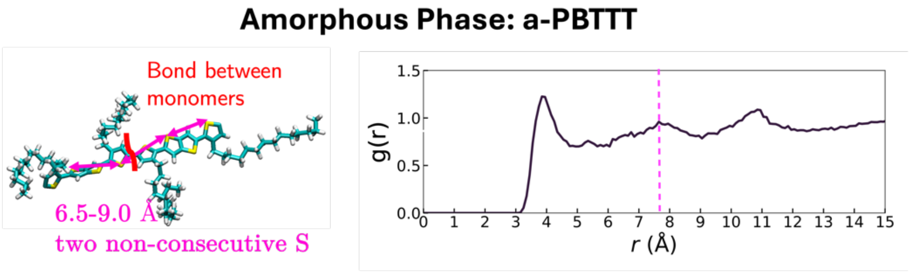

Figure S19 Radial distribution function (RDF) of a-PBTTT with the assignment of inter-chain peaks.

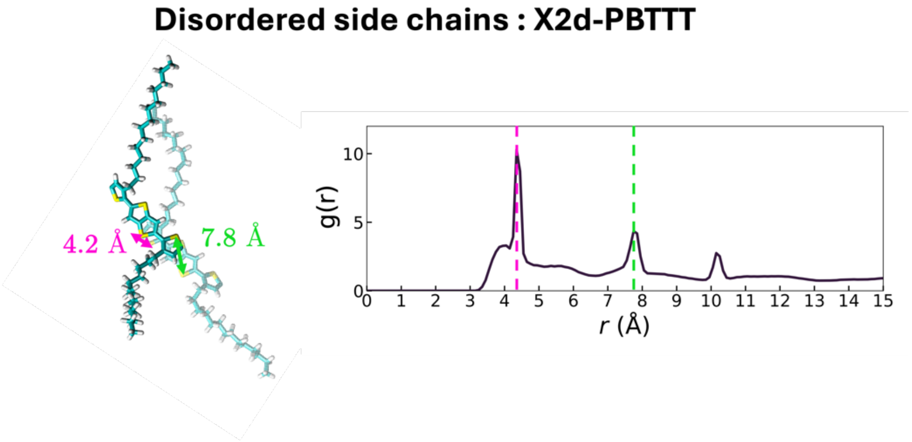

Figure S20 Radial distribution function (RDF) of X2d-PBTTT with the assignment of inter-chain peaks.

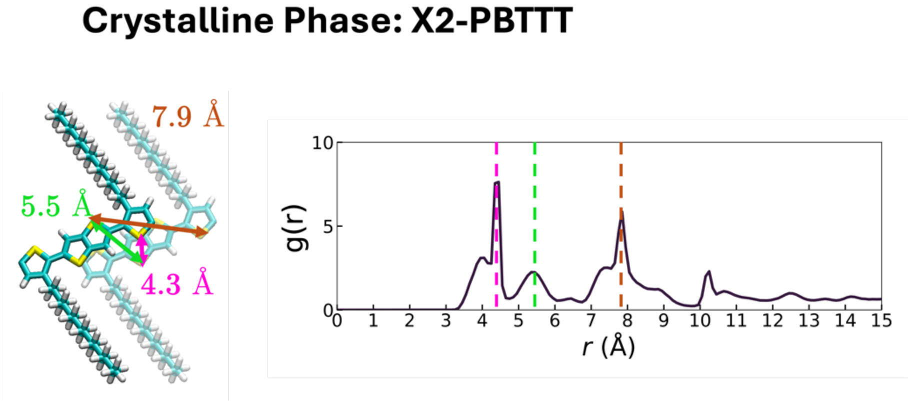

Figure S21 Radial distribution functions (RDF) of X2-PBTTT with the assignment of inter-chain peaks.

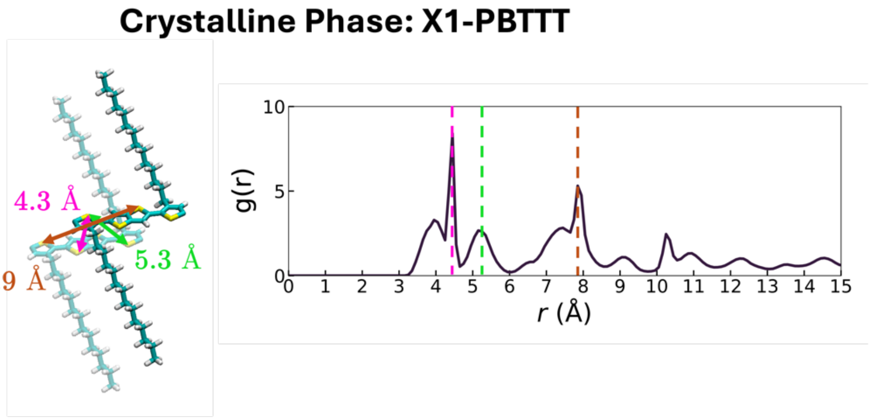
Crystalline Phase: X1-PBTTT

Figure S22 Radial distribution functions (RDF) of X1-PBTTT with the assignment of inter-chain peaks.

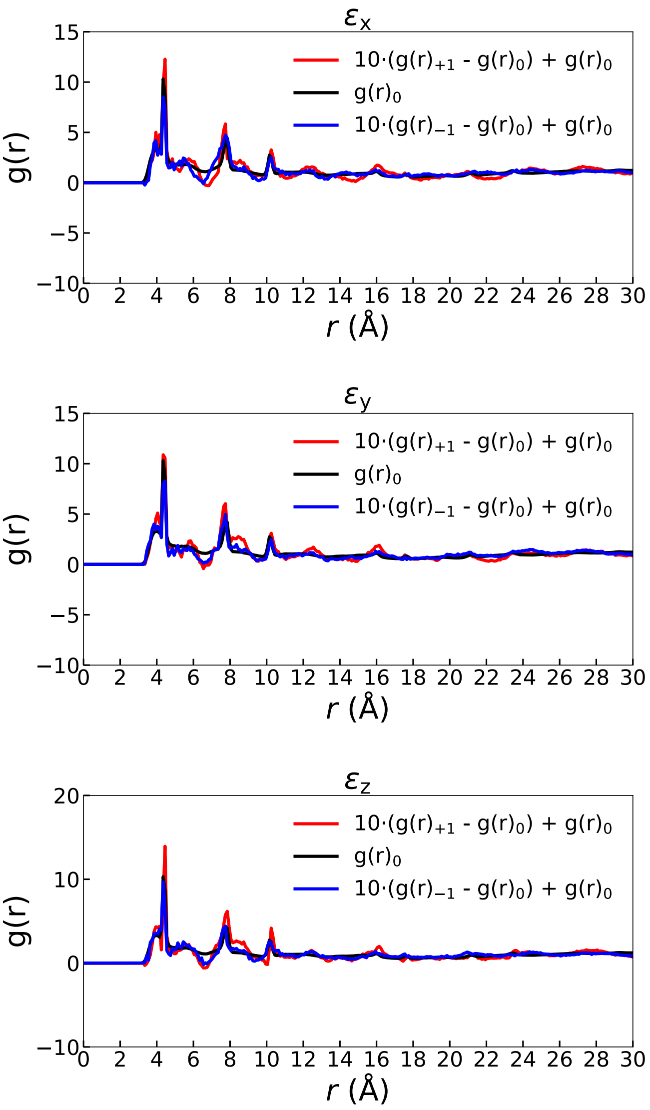

Figure S23 Radial distribution function, g(r), of X2d-PBTTT for ε=0%, ε=+1.0% and ε=-1.0% along the *X, Y* and *Z* axes. To highlight changes, in each plot is shown the $g(r)_0$ (black line) for ε=0%, and $10(\ g(r)_{\pm1}\ g(r)_0)+ g(r)_0$ for ε=+1.0% and ε=-1.0% (red and blue lines for ε=-1.0% and ε=+1.0%, respectively).

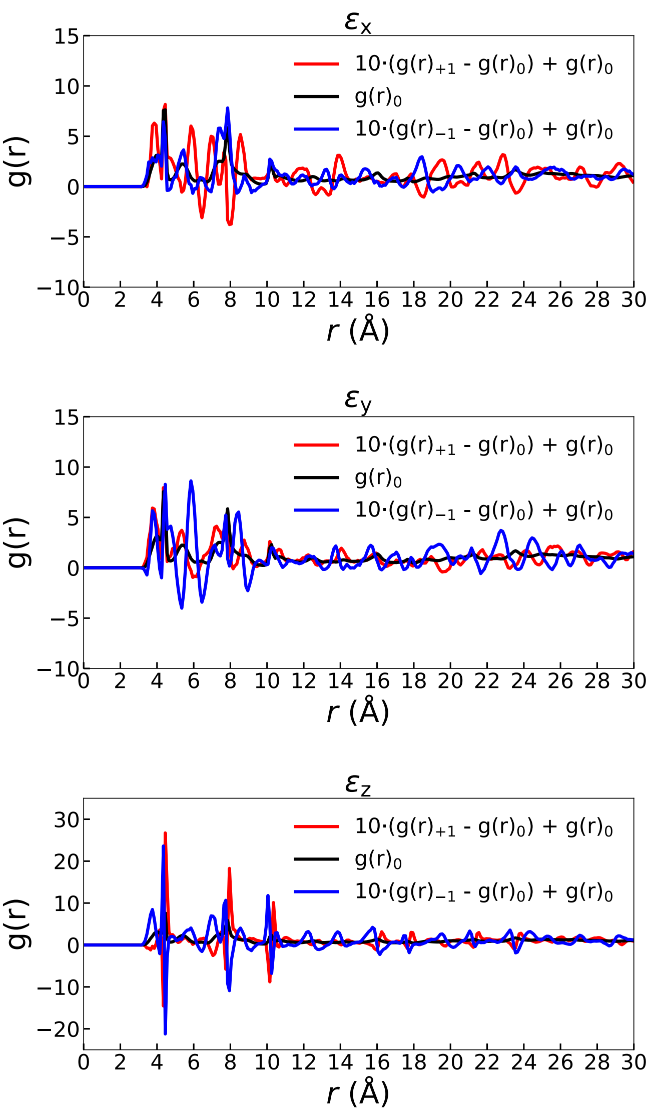

Figure S24 Radial distribution function, g(r), of X2-PBTTT for ε=0%, ε=+1.0% and ε=-1.0% along the *X, Y* and *Z* axes. To highlight changes, in each plot is shown the g(r)$_0$ (black line) for ε=0%, and 10(g(r)$_{\pm1}$ g(r)$_0$)+ g(r)$_0$ for ε=+1.0% and ε=-1.0% (red and blue lines for ε=-1.0% and ε=+1.0%, respectively).

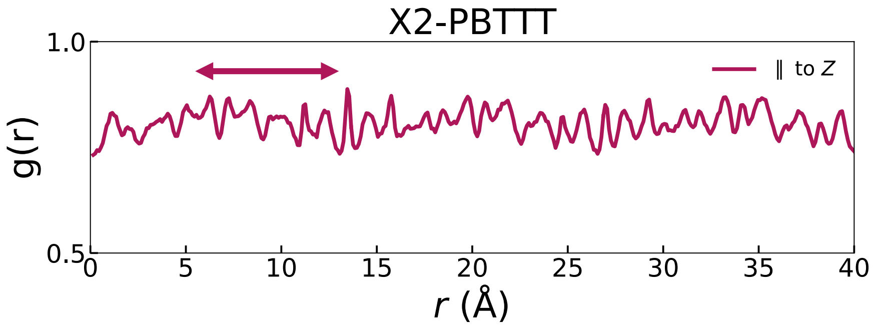

Figure S25 Radial distribution function g(r) of X2-PBTTT computed parallel to the backbone axis. The arrow highlights the periodic peaks corresponding to monomer lengths along the polymeric chain.

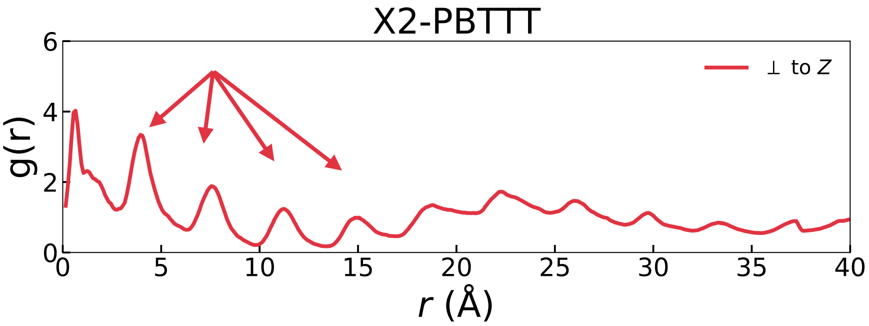

Figure S26 Radial distribution function g(r) of X2-PBTTT computed perpendicular to the backbone axis. Arrows point to the periodic peaks corresponding to π-stacking interaction among polymeric chains. The bump at above 25 Å correspond to the interlamellar planes.

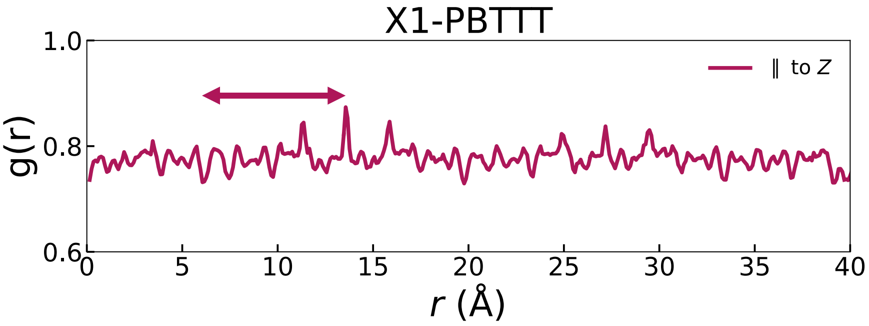

Figure S27 Radial distribution function g(r) of X1-PBTTT computed parallel to the backbone axis. The arrow highlights the periodic peaks corresponding to monomer lengths along the polymeric chain.

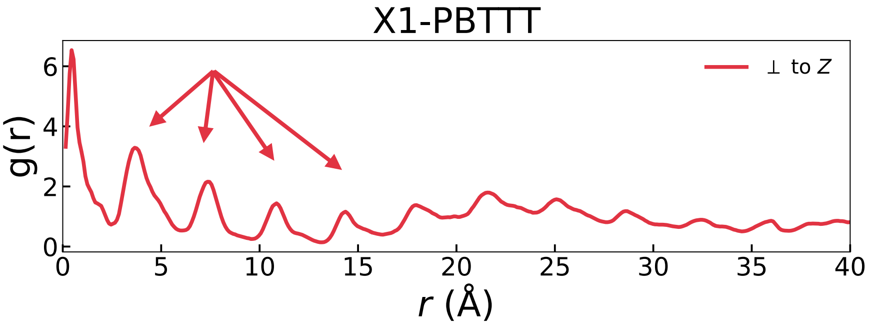

Figure S28 Radial distribution function g(r) of X1-PBTTT computed perpendicular to the *Z* axis. Arrows point to the periodic peaks corresponding to π-stacking interaction among polymeric chains. The bump above 25 Å correspond to the interlamellar planes.

SECTION 8. End-to-End distances distribution for IDTBT and PBTTT amorphous phases

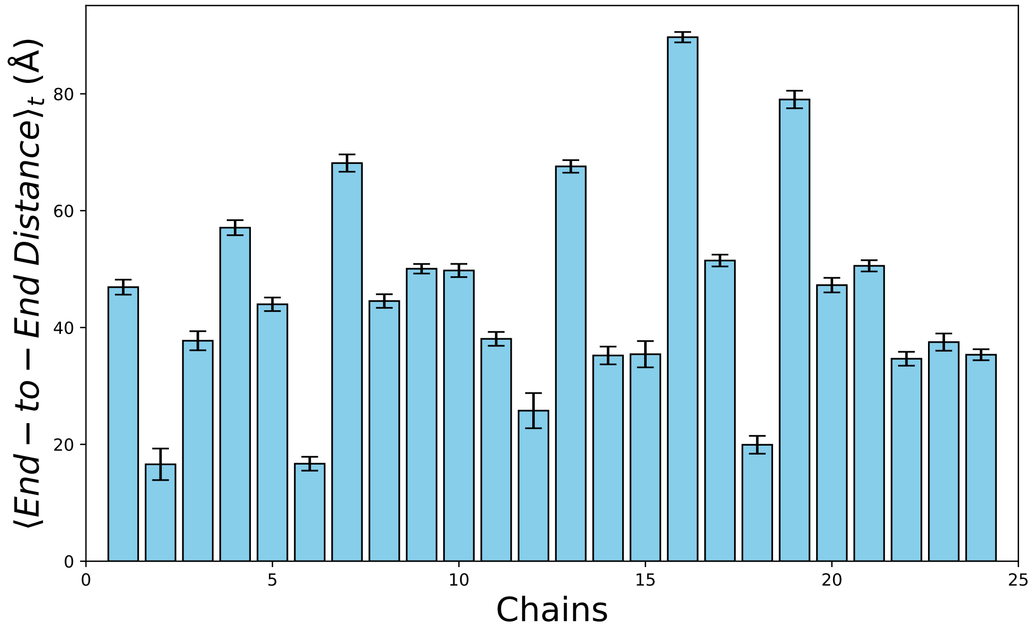

Figure S29 Time-averaged end-to-end distances of PBTTT chains in the amorphous phase, obtained from an NPT-equilibrated simulation. Each bar in the plot represents a single polymer chain (N chains = 24), with error bars indicating the standard deviation over time.

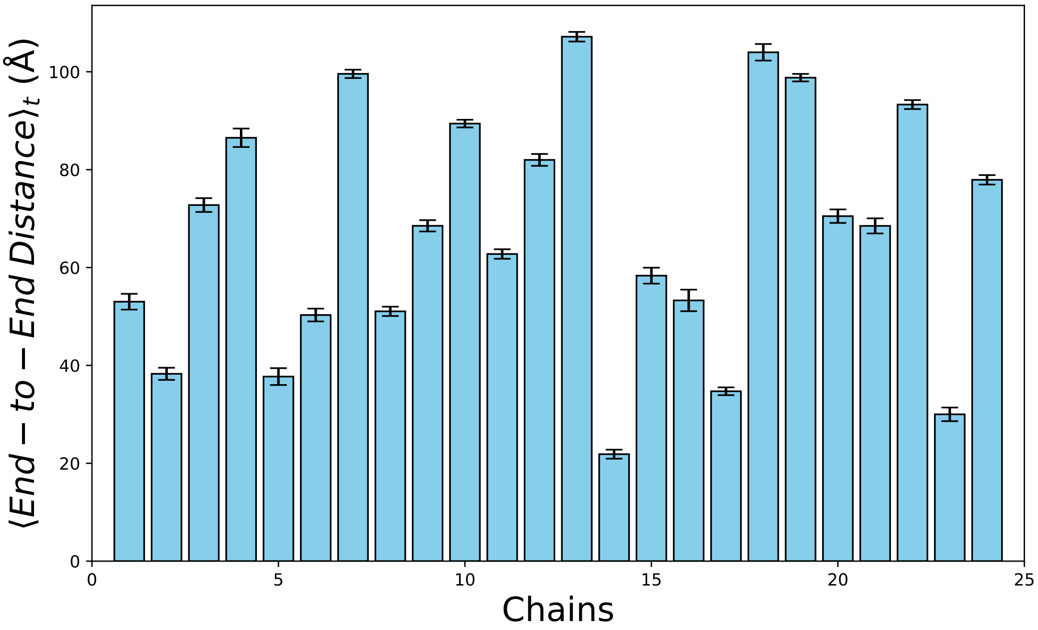

Figure S30 Time-averaged end-to-end distances of IDTBT chains in the amorphous phase, obtained from an NPT-equilibrated simulation. Each bar in the plot represents a single polymer chain (N chains = 24), with error bars indicating the standard deviation over time.

References

[1] Matta, M., Pereira, M. J.; Gali, S. M., Thuau, D., Olivier, Y., Briseno, A., Dufour, I., Ayela, C., Wantz, G., Muccioli, L. Unusual electromechanical response in rubrene single crystals. Material Horizons, 2018, **5**, 41-50